Cell Biol Toxicol (2012) 28:89–101
DOI 10.1007/s10565-011-9209-3

ORIGINAL RESEARCH

Toxicity of 6-hydroxydopamine: live cell imaging of cytoplasmic redox flux

Colette T. Dooley · Ling Li · Jaime A. Misler · Jane H. Thompson

Received: 28 July 2011 / Accepted: 20 December 2011 / Published online: 8 January 2012

Abstract Oxidative stress contributes to several debilitating neurodegenerative diseases. To facilitate direct monitoring of the cytoplasmic oxidation state in neuronal cells, we have developed roTurbo by including several mutations: F223R, A206K, and six of the mutations for superfolder green fluorescent protein. Thus we have generated an improved redox sensor that is much brighter in cells and oxidizes more readily than roGFP2. Cytoplasmic expression of the sensor demonstrated the temporal pattern of 6-hydroxydopamine (6-OHDA) induced oxidative stress in a neuroblastoma cell line (SH-SY5Y). Two distinct oxidation responses were identified in SH-SY5Y cells but a single response observed in cells lacking monoamine transporters (HEK293). While both cell lines exhibited a rapid transient oxidation in response to 6-OHDA, a second oxidative response coincident with cell death was observed only in SH-SY5Y cells, indicating an intracellular metabolism of 6-OHDA, and or its metabolites are involved. In contrast, exogenously applied hydrogen peroxide induced a cellular oxidative response similar to the first oxidation peak, and cell loss was minimal. Glucose deprivation enhanced the oxidative stress induced by 6-OHDA, confirming the pivotal role played by glucose in maintaining a reduced cytoplasmic environment. While these studies support previous findings that catecholamine auto-oxidation products cause oxidative stress, our findings also support studies indicating 6-OHDA induces lethal oxidative stress responses unrelated to production of hydrogen peroxide. Finally, temporal imaging revealed the sporadic nature of the toxicity induced by 6-OHDA in neuroblastoma cells.

Keywords Dopamine · Green fluorescent protein · Hydrogen peroxide · Oxidative stress · Redox · Neuroblastoma

Abbreviations

DTT	Dithiothreitol
GFP	Green fluorescent protein
GSH/GSSG	Glutathione/glutathione-disulfide ratio
NAC	*N*-acetyl cysteine
6-OHDA	6-Hydroxydopamine
PPP	Pentose phosphate pathway
RNS	Reactive nitrogen species
ROS	Reactive oxygen species
RLU	Relative luminescent units
roGFP	Redox sensitive green fluorescent protein
SEM	Standard error of the mean

Electronic supplementary material The online version of this article (doi:10.1007/s10565-011-9209-3) contains supplementary material, which is available to authorized users.

C. T. Dooley (✉) · L. Li · J. A. Misler · J. H. Thompson
Torrey Pines Institute for Molecular Studies,
11350 SW Village Parkway,
Port St. Lucie, FL 34987, USA
e-mail: cdooley@tpims.org

Introduction

Oxidative damage to proteins, DNA, and lipids is associated with a number of age-related neurodegenerative diseases including Alzheimer's and Parkinson's diseases (see Halliwell 2001; Uttara et al. 2009; Zhu et al. 2007; Zhou et al. 2008, for reviews). Reactive oxygen and nitrogen species (ROS and RNS) are generated as secondary products of normal metabolic and anabolic processes. While physiological levels of ROS regulate cell signaling and gene expression, excess production of ROS results in oxidative stress, which in turn leads to impaired cell function and ultimately to apoptosis or necrosis. Alterations in the cytoplasmic redox equilibrium are reflected in changes in the ratio of reduced to oxidized thioredoxin and/or the ratio of glutathione to glutathione-disulfide (GSH/GSSG) and can be used as an indicator of the cellular redox state (Hwang et al. 1992; Liu et al. 1996).

Redox-sensitive green fluorescent proteins (roGFP) have enabled real-time visualization of changes in intracellular oxidation states (Dooley et al. 2004; Hanson et al. 2004). These indicators have two surface-exposed cysteines placed on adjacent β-strands close to the chromophore. The ratios of emitted fluorescence after excitation at 400 and 490 nm provide an indication of the degree of oxidation and thus the environmental redox potential, while remaining independent of the indicator concentration or its absolute optical sensitivity. The original sensor, roGFP2, was used to detect ROS generation during the oxidative burst in macrophages. However, it less successful at detecting changes in redox equilibria in situations where less severe oxidative events are known to occur, such as during hypoxia or glucose deprivation. The reaction of the sensor was limited by the rate of deprotonation of the thiol prior to oxidation reaction. To correct this, a positive charge (lysine) was placed in roGFP2 proximal to cysteine 204, and while improved, the reaction rate was not sufficiently increased (Dooley et al. 2004). Reactivity of roGFP1 was later improved by inclusion of arginine in place of lysine (Cannon and Remington 2006). More recently, an alternative method to improve the sensitivity and response rate was to fuse roGFP2 to the enzyme glutaredoxin (Gutscher et al. 2008), and although this sensor proved very efficient, its larger size is not ideal. Another fluorescent indicator that is a fusion of fluorescent protein and sensor is HyPER, which combines a circular permuted YFP and the H_2O_2 sensing protein OxyR (Belousov et al. 2006).

In the present study, we have modified roGFP2 by mutating phenylalanine 223 to arginine (F223R) and alanine 206 to lysine (A206K) and have also included six of the seven mutations of the more robust superfolder GFP (Pedelacq et al. 2006) (supplemental Fig. 1). These mutations have been combined to generate a redox GFP (roTurbo) that is much brighter in cells and oxidizes more readily than roGFP2.

Although oxidative stress is known to occur in Parkinson's and Alzheimer's diseases, it remains unclear as to whether oxidative stress is an inherent part of the pathophysiology of the disease or is a consequence of toxic events within dying neurons (reviewed in Blum et al. 2001). 6-Hydroxydopamine (6-OHDA) is commonly used in experimental models of Parkinson's disease in vitro and in vivo. This compound destroys nigral dopaminergic neurons and depletes the striatum of the neurotransmitter dopamine, and 6-OHDA may be an endogenous neurotoxin (Andrew et al. 1993; Curtius et al. 1974; Senoh et al. 1959). Several studies with cultured cells have indicated an extracellular mechanism for 6-OHDA toxicity. It is known to generate ROS, however, the molecular mechanism by which 6-OHDA induces oxidative injury in vivo has not been fully elucidated (Callio et al. 2005; Chalovich et al. 2006). Dopamine and 6-OHDA are unstable and undergo rapid auto-oxidation to generate hydrogen peroxide, quinones, and semiquinones accordingly, several groups have suggested that ROS generated by auto-oxidation are the main cause for toxicity (Blum et al. 2000; Clement et al. 2002; Jiang et al. 2008; Soto-Otero et al. 2000). Hydrogen peroxide produced by auto-oxidation of 6-OHDA may react within the cell with ferrous iron to generate hydroxyl radicals, but the involvement of Fe^{2+} in the neurotoxicity of 6-OHDA has not been definitively established (Soto-Otero et al. 2000). More recently, the quinone metabolite has been attributed with cytotoxicity (Izumi et al. 2005; Saito et al. 2007).

We now have the capability of monitoring the cytoplasmic redox state of neuronal cells in response to 6-OHDA and can thereby confirm the relationship between oxidative stress and toxicity. In the present study, we have used the new redox sensor to determine the initiation and progression

of redox responses of neuroblastoma SH-SY5Y cells in response to this toxic catecholamine and establish whether oxidative stress correlates with or heralds cell death.

Materials and methods

Materials Aldrithiol, hydrogen peroxide, and 6-hydroxydopamine hydrobromide were purchased from Sigma-Aldrich (St Louis, MO).

Gene cloning Eight amino acid mutations were incorporated into roTurbo using eight individual site-directed mutagenesis reactions (Stratagene, Santa Clara, CA). The mutated constructs were cloned into pBAD (Invitrogen, Carlsbad, CA) expressed in JM109 bacteria and purified as described below. For expression in mammalian cells, the constructs were subcloned into pcDNA3 (Invitrogen) using BamHI and EcoRI restriction sites.

In vitro studies roGFP constructs were subcloned into pRSET-B (Invitrogen) using BamHI and EcoRI restriction sites. The construct was expressed in the BL21 strain of *Escherichia coli* and purified by nickel affinity chromatography. Isolated protein was reduced with 20 mM dithiothreitol (DTT), which was subsequently removed using Centri-spin 20 columns (Princeton Separations Inc., Adelphia, NJ). Fluorescence excitation scans (350–500 nm, 2.5-nm bandwidth) were performed on a Safire spectrofluorometer (Tecan, Mannedorf, Switzerland), with emission at 530±10 nm. Assays were performed in duplicate in 100 μL volumes using 1 μM protein in HEPES buffer pH 7.4 and incubated for 1 h. To determine whether roTurbo was more sensitive to oxidation, excitation ratios were determined for the oxidation roTurbo and SF-roGFP2 (the original redox sensor with superfolder mutations) for a range of concentrations of H_2O_2. To determine 6-OHDA was not binding directly to roTurbo, excitation spectra of roTurbo reduced and oxidized alone were compared with those in the presence of 100 μM 6-OHDA. Full oxidation was confirmed via overlap of spectra to roTurbo oxidized with aldrithiol (100 μM). Full reduction of roTurbo following oxidation with 6-OHDA was determined with excess DTT (10 mM). Oxidation of roTurbo was monitored in DMEM media (no phenol red) and HEPES over 2 h. Increased oxidation rates in media in the presence of 6-OHDA were determined using 100, 300, and 500 μM concentrations.

Cell culture and transfection SH-SY5Y cells were cultured in medium consisting of 45% (*v/v*) MEM, 45% F12-Ham (Hyclone, Logan, UT), 10% fetal bovine serum (FBS), 1,000 μg/ml each penicillin and streptomycin (Invitrogen), and 2 mM glutamax (Invitrogen). HEK293 cells were cultured in high glucose (4.5 g/L) DMEM (Invitrogen), 10% FBS, and 1,000 μg/ml each penicillin and streptomycin (Invitrogen). RoTurbo was expressed in SH-SY5Y or HEK 293 cells using modified pCDNA3 as the expression vector and Fugene (Roche Applied Science, Indianapolis, IN) as the transfection reagent. Cells were seeded at 5×10^4 cells per well onto laminin-coated glass plates (Greiner Bio One, Monroe, NC) 24 h prior to transfection.

Live cell imaging Two hours prior to imaging, the cell culture medium was replaced with phenol red-free assay medium (100 μl/well in 96-well plates. Assay medium contained DMEM/F12 (1:1 ratio) with 3.1 g/L glucose (BD Diagnostics MD) and 10% FBS). A stock solution of 6-OHDA was prepared in diluted to 100 μM in assay media. Glucose starvation was performed by incubating in glucose-free DMEM (Mediatech, Manassas, VA) containing 10% FBS. Imaging experiments were carried out on a Zeiss Axiovert Microscope equipped with a scanning stage, an incubation chamber, an ultra-high speed Lambda DG-4 wavelength switcher, and an Axiocam CCD camera (Zeiss, Gottingen, Germany) all controlled by Axiovision software 4.8. Cells were maintained during imaging at 37°C in a 5% CO_2 atmosphere. Emission (530 nm) was captured after excitation at 390 and 485 nm using 390 DF18 and 485DF20 filters for excitation, 531DF22 filter for emission, and a GFP Dichroic FF495 filter (Semrock, Rochester, NY). Exposure times were 150 ms for 485 nm and 600 ms for 390 nm. Images were background-corrected by manual selection of background regions. The excitation ratios were calculated as $Em_{530\ nm}=(Ex_{390nm}-\text{background})/(Ex_{485nm}-\text{background})$. Regions were selected to image individual cells and ratios were obtained for 10–14 cells per experiment. Figures show representative data from one of two experiments, with each experiment repeated in quadruplicate. Untreated SH-SY5Y cells did not exhibit oxidative stress for up to

12 h when cultured in 96-well plates. Cells moved freely throughout the 12- to 15-h experimental period, as cells in the field of view changed between time intervals.

Addition of compounds Cells were treated with 6-OHDA or H_2O_2 following capture of three to five image frames. For cell treated with 6-OHDA (100 μM) stock solution (40 mM) was prepared in 100% ethanol and diluted to 100 μM in assay media. H_2O_2 solutions (100 μM) were prepared from concentrated solution daily. Cells were pretreated with *N*-acetylcysteine (10 mM) for 2 h prior to addition of oxidant. For glucose deprivation experiments, cell media was changed from high glucose media (3.1 g/L) to glucose-free media 2 h before addition of test compounds.

Cell viability estimations Cell viability was determined using two assays; the first was integral to the redox experiment, it monitored cell number by counting physical disappearance of cells from the images. The number of GFP-expressing cells was determined for all images and was captured using particle analysis with Image J 1.42 software (NIH) for images obtained at 490 nm. To ensure that only healthy cells were counted, rounded cells were eliminated from the count by creating and counting masks with pixel size greater than 300 and circularity range of 0–0.5. Percentages were calculated using the number of cells present at the zero time point. The second assay measuring ATP was used to verify cell viability estimations detects dead and dying but intact cells. CellTiter Glo (Promega, Madison, WI) at 100 μl/well was added, and luminescence was detected on a Tecan Safire2. Relative luminescent units were expressed as a percentage of the zero time-point immediately after CellTiter Glo addition. A third assay using nuclear staining was used to verify cell death. One hour prior to the termination of each experiment, 0.1 mg/ml 4, 6-diamidino-2-phenylindole (DAPI) was added to the wells. Images were acquired at an excitation wavelength of 390 nm using excitation filter 390 DF18 and an emission wavelength at 531 nm. Images were analyzed and DAPI nuclear staining quantified using Image J software.

Statistical analyses Data are presented as mean±standard error of the mean (SEM) and are representative of four independent experiments unless otherwise stated. Statistical analyses for protein oxidation or cell death were analyzed using one-way ANOVA, and significant effects were further analyzed using either Dunnett's post hoc test for comparisons to the initial zero time-point, or by Tukey's post hoc test for comparison between time points. Statistical analyses were performed with Prism software version 5.00 (GraphPad, San Diego, CA). Significance levels are indicated as ns $P>0.05$, *P value 0.01–0.05, **P value 0.001–0.01, ***$P<0.001$).

Results

Improved redox green fluorescent protein

The response rate of roGFP2 was improved after site-directed mutagenesis of F223R and A206K. The protein was made brighter by inclusion of six of the seven mutations of the superfolder GFP (Pedelacq et al. 2006), i.e., S30R, Y39N, F99S N105T, I171V, and V163A. These mutations combined to yield a new redox GFP (roTurbo) that is much brighter in mammalian cells (Fig. 1a) and oxidizes more readily than the non-mutated roGFP2 (Fig. 1b). The redox potential of roTurbo (E'=−275±2 mV) was found to be slightly higher for roGFP2 (E'=−284±7 mV) (Dooley et al. 2004). Auto-oxidation of 6-OHDA in DMEM and generation of H_2O_2 and *p*-quinone were demonstrated (supplementary Fig. 2). To ensure that 6-OHDA did not interact directly with the GFP sensor, roTurbo was oxidized in the presence of 6-OHDA in cell-free experiments using either HEPES buffer or phenol-free cell DMEM; the protein exhibited complete oxidation in the presence of 6-OHDA and was subsequently fully reduced by DTT (Fig. 1c). Oxidation was more rapid in DMEM than in HEPES buffer, but the maximal ratios achieved were similar to those without 6-OHDA (Fig. 1d). Initial ratios were slightly higher in the presence of 6-OHDA than in buffer, presumably due to absorption at 480 nm by oxidation products (Blum et al. 2000; Soto-Otero et al. 2000).

Cytoplasmic redox responses to 6-OHDA

We used roTurbo to compare the oxidative responses to 6-OHDA in cells with and without monoamine transporters (SH-SY5Y and HEK293, cells respectively) (Miller et al. 2001). Data for untreated controls are presented in Supplemental Fig. 3. HEK293 cells are

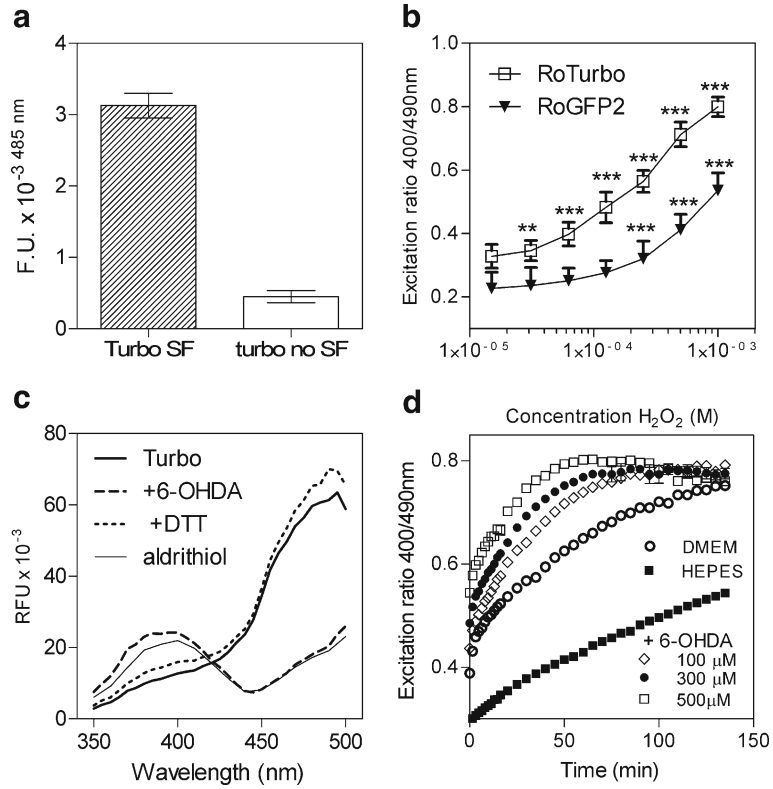

Fig. 1 Characteristics of roTurbo a modified redox sensor. **a** When expressed in cell cytoplasm the fluorescence of roTurbo containing superfolder mutations (Turbo SF) is greater than the redox protein with only the F223R mutation (Turbo no SF). In vitro studies of free protein; **b** roTurbo oxidizes more rapidly than redox-GFP. Excitation ratios for the oxidation of SF-roGFP2 and roTurbo by H_2O_2 (points are represented as mean±SD n=4 of two protein preparations with two replicates) for 1 h. **c** Oxidation of roTurbo in the presence of 6-OHDA is complete and reversible. Excitation spectra of roTurbo reduced and oxidized alone or in the presence of 100 µM 6-OHDA and subsequent reduction with DTT (10 mM) or oxidation with aldrithiol (100 µM). **d** Oxidation rate increases with increasing concentrations of 6-OHDA. Excitation ratios for roTurbo in HEPES buffer, DMEM, and DMEM with the indicated concentrations of 6-OHDA

not expected to display intracellular responses to dopamine or 6-OHDA (Jiang et al. 2004). Two distinct oxidation responses were observed in SH-SY5Y cells: excitation ratios in the whole population rose within 30 min (Fig. 2a), decreased, and then increased for a second time after approximately 4 h. The first oxidative response was transitory; cells recovered from the oxidative insult, and excitation values returned to baseline within 2 h. The second oxidative response was characterized by individual cells responding at distinct timepoints. Furthermore, this oxidative rise was associated with cell death. For this reason, we present the data as individual ratios rather than averaged ratios. These cells displayed a maximal oxidative response as they became round in shape and then were subsequently lost (see Figs. 2b and 3a and images in Fig. 4).

The response of HEK293 cells to 6-OHDA differed from that observed in SH-SY5Y cells. While HEK293 cells exhibited a similar first transitory excitation response, which reached a maximum in 1–2 h (Fig. 3e, image in Fig. 4), they did not display the secondary oxidative response. A singular oxidative response to 6-OHDA was also found in HeLa cells, another cell line lacking monoamine transporters (data not shown).

Cytoplasmic redox responses to H_2O_2

It is has been reported by several laboratories that 6-OHDA-induced oxidative stress and toxicity are mediated through ROS, namely hydrogen peroxide production. To test this, we compared the responses of SH-

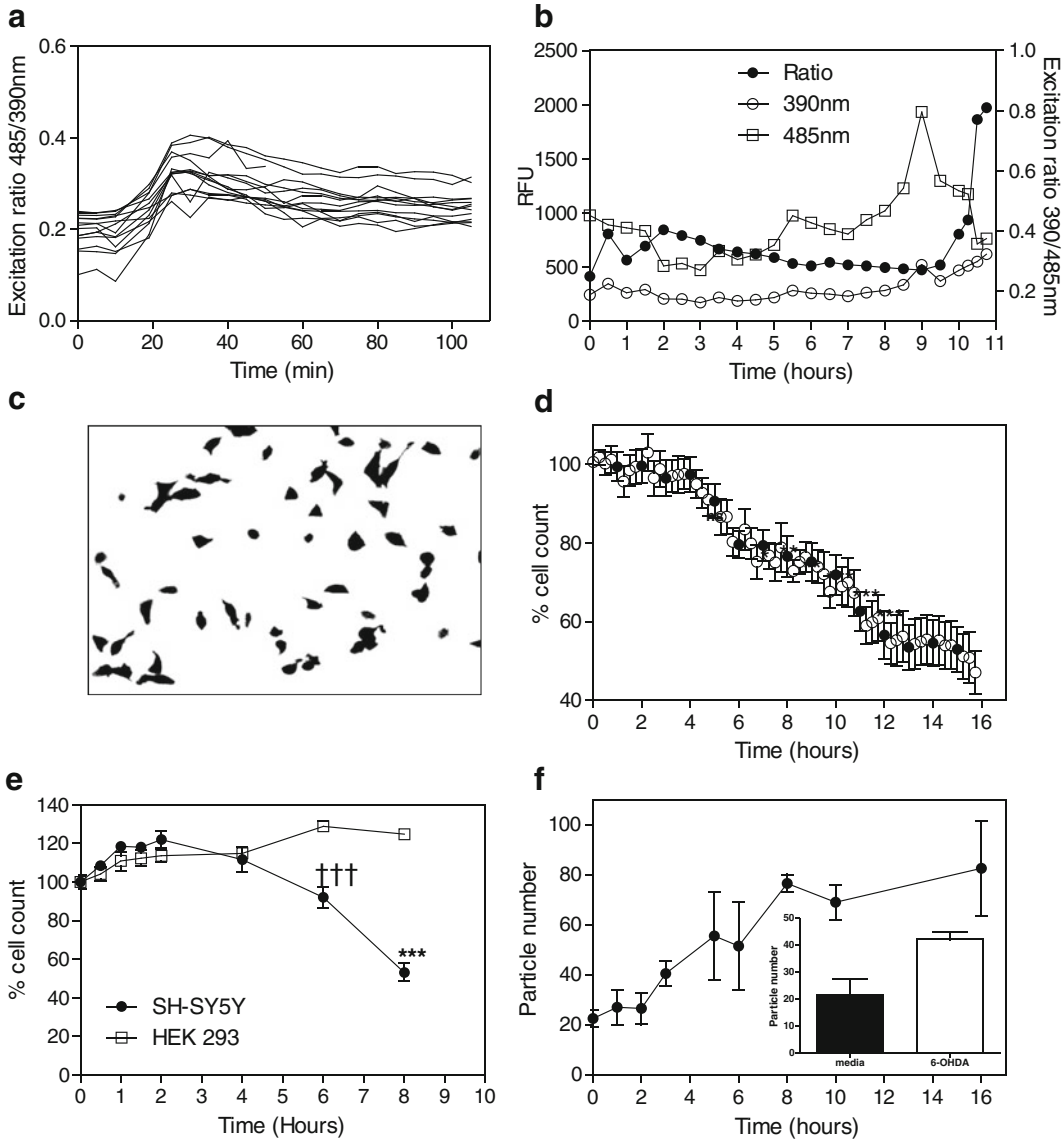

Fig. 2 Monitoring oxidation and toxicity 6-OHDA in SH-SY5Y using cytoplasmic roTurbo. Conditions for imaging are detailed in Materials and methods. **a** Early oxidation responses to 6-OHDA (100 μM).. Each line represents the excitation ratio observed within an individual cell taken at 5-minute intervals. In later graphs these points are compressed and appear as a single pointed peak. **b** Oxidation responses of a single cell exposed to 100 μM 6-OHDA. Fluorescence values for each of the two excitation wavelengths and the corresponding ratios are presented. **c** Example of mask from Image J cells used to identify viable cells for cell population estimates. **d** Cell count following treatment with 6-OHDA (100 μM). Cell numbers drop to significantly by six hours (P =0.01-0.05) and is highly significant (P<0.001) at 10 hours (points represent mean± SEM n=11). (● time-points used in statistical analyses). **e** Comparable time scales are obtained when cell viability is monitored by reduction in ATP production, concentrations were significantly lower at 8 hours (***, P<0.001) compared to the zero time point. The six hour time point differed significantly from the 2 hour time point (†††, P<0.001, mean±SEM n=4). HEK293 cell numbers are not effected by 6-OHDA. (f) Likewise cell death induced by 6-OHDA treatment and monitored by DAPI staining of DNA showed a similar timeframe (mean±SD n=2). Insert: DAPI stained cells±6-OHDA (3 hours, mean±SD n=3)

SY5Y cells and HEK293 to exogenous H_2O_2. No significant increase in excitation ratio was observed when cells were treated with 10 μM H_2O_2, which is the concentration estimated to result from auto-oxidation of 100 μM dopamine (Clement et al. 2002); Saito et al. 2007 reported 6-OHDA produced approximately

50 μM H_2O_2 ; we estimated 100 μM H_2O_2 (see Supplemental Fig. 2). Addition of 100 μM H_2O_2 induced the rapid initial transitory response but no secondary increase in excitation ratio; the oxidative response was comparable to those induced by 6-OHDA in cells without monoamine transporters. The responses to H_2O_2 were equivalent in both SH-SY5Y and HEK293 cell lines (Fig. 3c, g; images in Fig. 4).

Cell toxicity induced by 6-OHDA but not by H_2O_2

By monitoring fluorescence directly, a recurrent estimate of cell numbers throughout the experimental period was possible. Using particle analysis software in Image J, masks of images of fluorescent cells using size and circularity parameters distinguished live from dead and dying cells. Live cell numbers were calculated for each image in the experiment (Fig. 2c–d). The number of SH-SY5Y cells treated with 6-OHDA decreased beginning at 4 h post-treatment while untreated cells showed no significant change in cell number over 12 h (Fig. 2d). Toxicity in 6-OHDA-treated cells was statistically significant from untreated cells by 6 h and plateaued at 50% cell death in 12 h. Our estimations of cell viability and cell loss yielded comparable results to those using the CellTiter-Glo luminescent assay (Fig. 2e) and cell death by DAPI labeling of nuclear DNA (Fig. 2f). DNA staining by DAPI can only occur when the cell membrane is compromised and the dye can enter the cell. Image counting as we describe herein could have cell numbers drop due to cells leaving the image view rather than cell death, and the CellTiter-Glo luminescent assay may indicate reduced cell metabolism but not prove cell death; DNA staining however provides proof of cell death. Since all three assays exhibited similar timeframes for cell number decline, we can conclude the cell loss we are observing in our images corresponds with cell death.

HEK293 cells showed no signs of toxicity when treated with 6-OHDA (Fig. 3h). Neither cell line exhibited a decline in cell number when treated with H_2O_2 (Fig. 3d, h) over a 12-h incubation period. Our results are consistent with those of Izumi et al. (2005) and Saito et al. (2007) who found in SH-SY5Y and PC12 cells respectively that extracellular catalase could inhibit hydrogen peroxide toxicity but not that of 6-OHDA.

Inhibition of oxidative and toxic responses by *N*-acetyl-cysteine

Treatment of either cell line with *N*-acetyl cysteine (NAC) prior to 6-OHDA addition prevented oxidation (Fig. 3b, f, and images in Fig. 4) and cell loss (Fig. 3d, h; images in Fig. 4). Using liquid chromatography mass spectrometry, we did not identify direct interaction between 6-OHDA and NAC in DMEM. We did identify the adduct in H_2O following either 2-h (14%) or 24-h (50%) incubation (Supplemental Fig. 4a–c). Pretreatment with NAC also fully inhibited responses to 100 μM H_2O_2; no changes in either redox state or cell viability were observed over 12 h (data not shown).

Glucose deprivation enhances redox responses and toxicity

Glucose metabolism through the pentose phosphate pathway contributes to the production of high levels of glutathione and thus to the maintenance of a reducing environment (Delgado-Esteban et al. 2000; Isaev et al. 2008). The relationship between D-glucose availability and oxidative stress was tested by monitoring the cellular response to 6-OHDA in glucose-free conditions. Control cultures survived a 12-h period in glucose-free medium mented with 10% serum; thereafter, they exhibited a rapid decline in number that was accompanied by a maximal change in cytoplasmic excitation ratio. All subsequent experiments were performed over 12 h or less. Cell media was changed from high glucose media (3.1 g/L) to glucose-free media 2 h before addition of test compounds. Glucose deprivation was associated with a dramatically increased redox response to 6-OHDA (Fig. 5, images in Fig. 6). The excitation ratios for the first oxidation peak are higher, and ratios never fully reduced to baseline values before the second increase in oxidation occurs. The period between oxidative stress and cell loss was lengthened. Cells rounded and numbers decreased throughout the incubation period following addition of 6-OHDA, and cells ceased regular movement within 2–3 h. Pretreatment of cells with NAC did not fully inhibit cytoplasmic oxidation but did prevent cell loss. Control experiments demonstrated NAC alone did not induce oxidative stress or cell death in glucose-starved cells.

HEK293 cells were more sensitive to glucose deprivation than SH-SY5Y cells; toxicity was observed

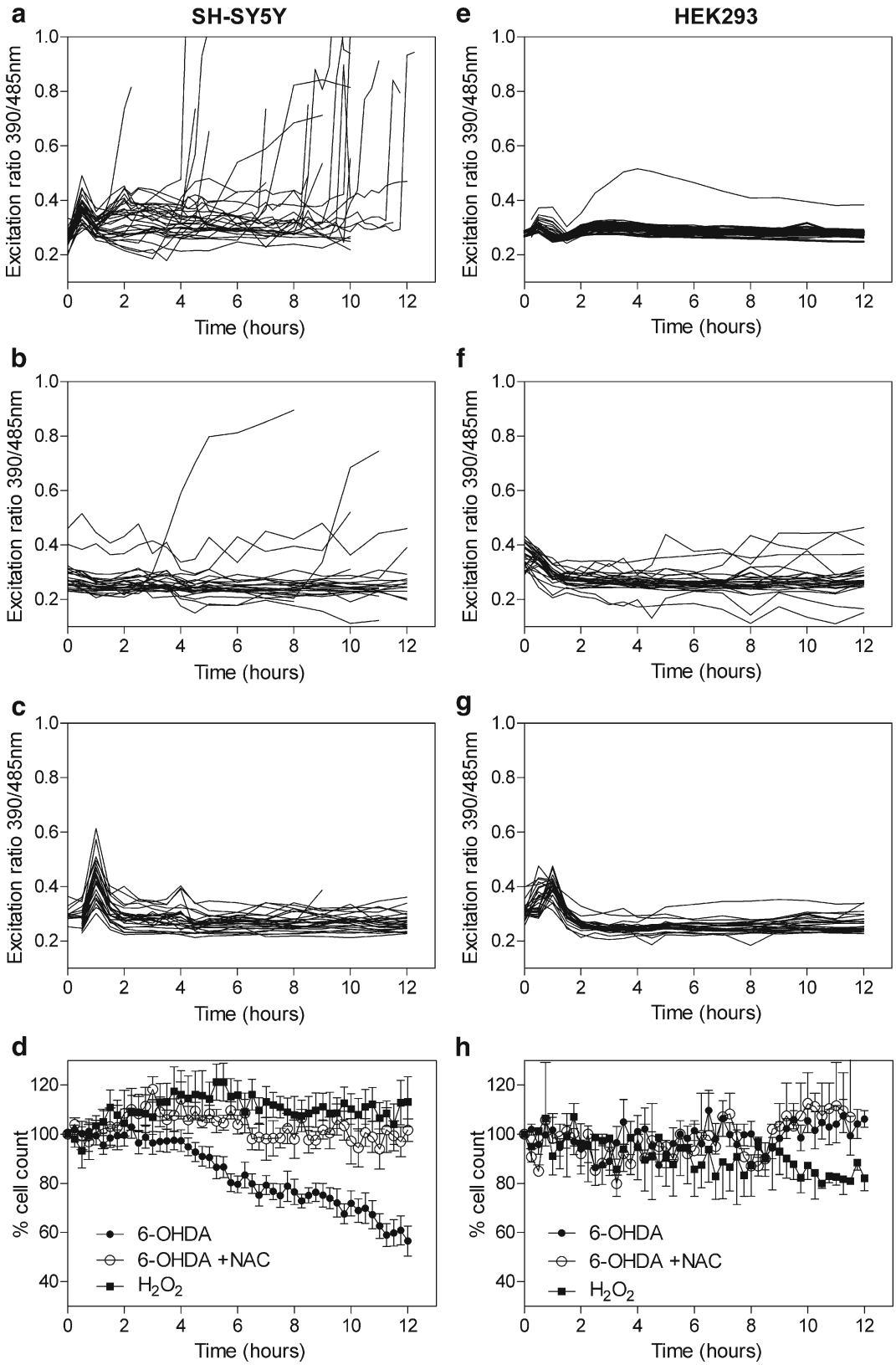
a
SH-SY5Y
e
HEK293
b
f
c
g
d
h
Excitation ratio 390/485nm
Time (hours)
% cell count
6-OHDA
6-OHDA +NAC
H2O2

◀ **Fig. 3** Oxidative stress and toxicity in SH-SY5Y cells induced by 6-OHDA differs from H_2O_2 in cells lacking monoamine transporters (HEK293). Conditions for imaging are detailed in "Materials and methods." Excitation ratios of cells treated with **a** 6-OHDA (100 μM), **b** 6-OHDA+10 mM NAC, and **c** H_2O_2 (100 μM). Identical treatments for HEK 293 cells are shown in *graphs* (**e**–**g**). *Graphs* represent the excitation ratios obtained for 20–30 individual cells from two experiments, however, each experiment repeated in quadruplicate. Cell viability studies **d** SH-SY5Y and **h** HEK293. Data are presented as averages and SEMs ($n \geq 4$). Graphs for untreated cells are provided in supplemental material

within 10 h. Treatment with 6-OHDA under glucose-free conditions raised the cytoplasmic redox values, but few cells recovered from the insult. Ratios did not return to baseline values as had been observed in previous experiments. Catastrophic toxicity occurred at 5–6-h incubation; cells were near maximal excitation ratios associated with cell death. Cell numbers did not drop in this set of experiments, but cell viability was clearly compromised by 6 h; cells contained a high number of vesicles, ceased regular movements, and shrank; a different mode of cell death was apparent. Pretreatment with NAC inhibited the initial oxidation response but not the catastrophic toxicity at 6 h.

Discussion

In this study, an improved redox-sensitive GFP (roTurbo) capable of real-time monitoring of the oxidative stress revealed differences in responses to 6-OHDA in cells expressing or lacking monoamine transporters. Additionally, direct estimations of cell viability allowed us to discriminate which of the oxidative responses correlated with cell toxicity. The original redox GFP, roGFP2, was improved in both expression efficiency and sensitivity to oxidation. Although roGFP2 and roTurbo use the same sensing mechanism, the increased intracellular fluorescence and improved response rate of roTurbo enabled us to conduct experiments that had not been possible with roGFP2. Exposure of the neuroblastoma cell line SH-

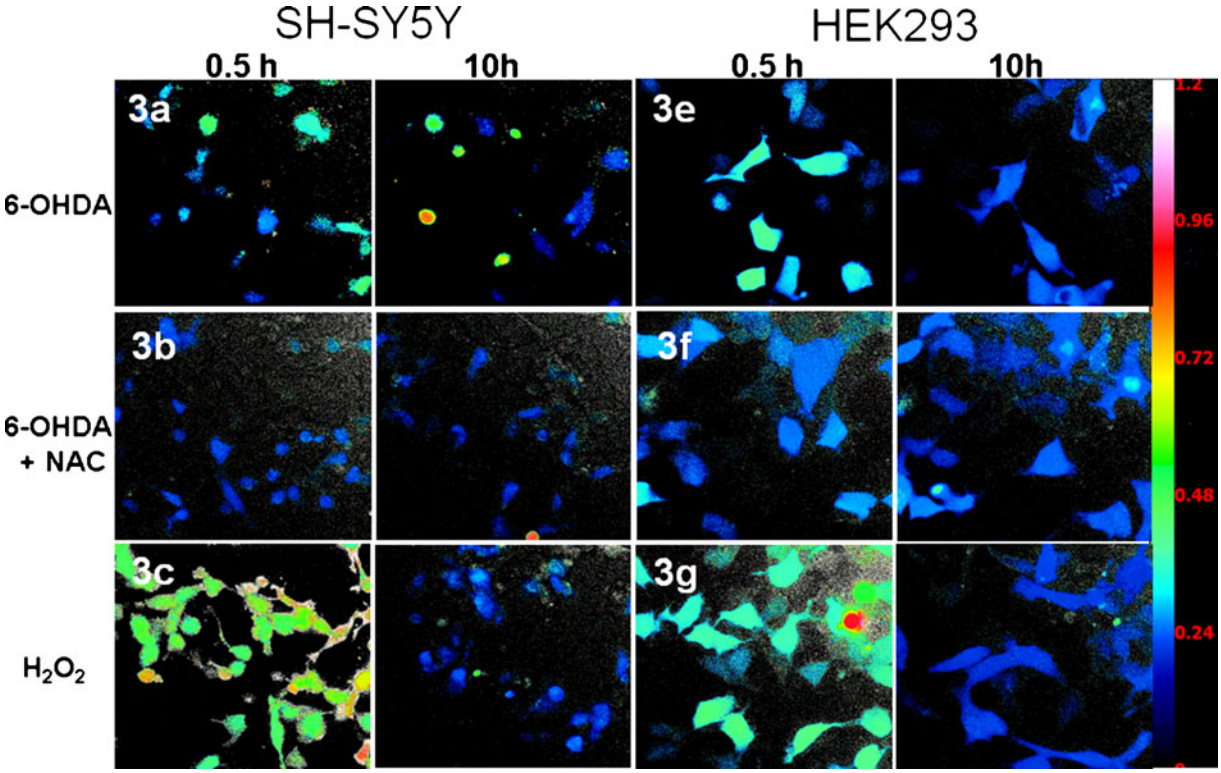

Fig. 4 Images for excitation ratios during cellular oxidative stress induced by 6-OHDA in SH-SY5Y and HEK293 cells. Images are from data graphed in Fig. 3 and have the same labels; they are presented as one quarter of the field observed and represent the 0.5- and 10-h time points. SH-SY5Y cells expressing roTurbo treated with (*3a*) 100 μM 6-OHDA, (*3b*) 6-OHDA+10mM NAC (*3c*) 100 μM H_2O_2, or HEK293 treated with (*3e*) 6-OHDA, (*3f*) 6-OHDA+NAC or (*3g*) H_2O_2

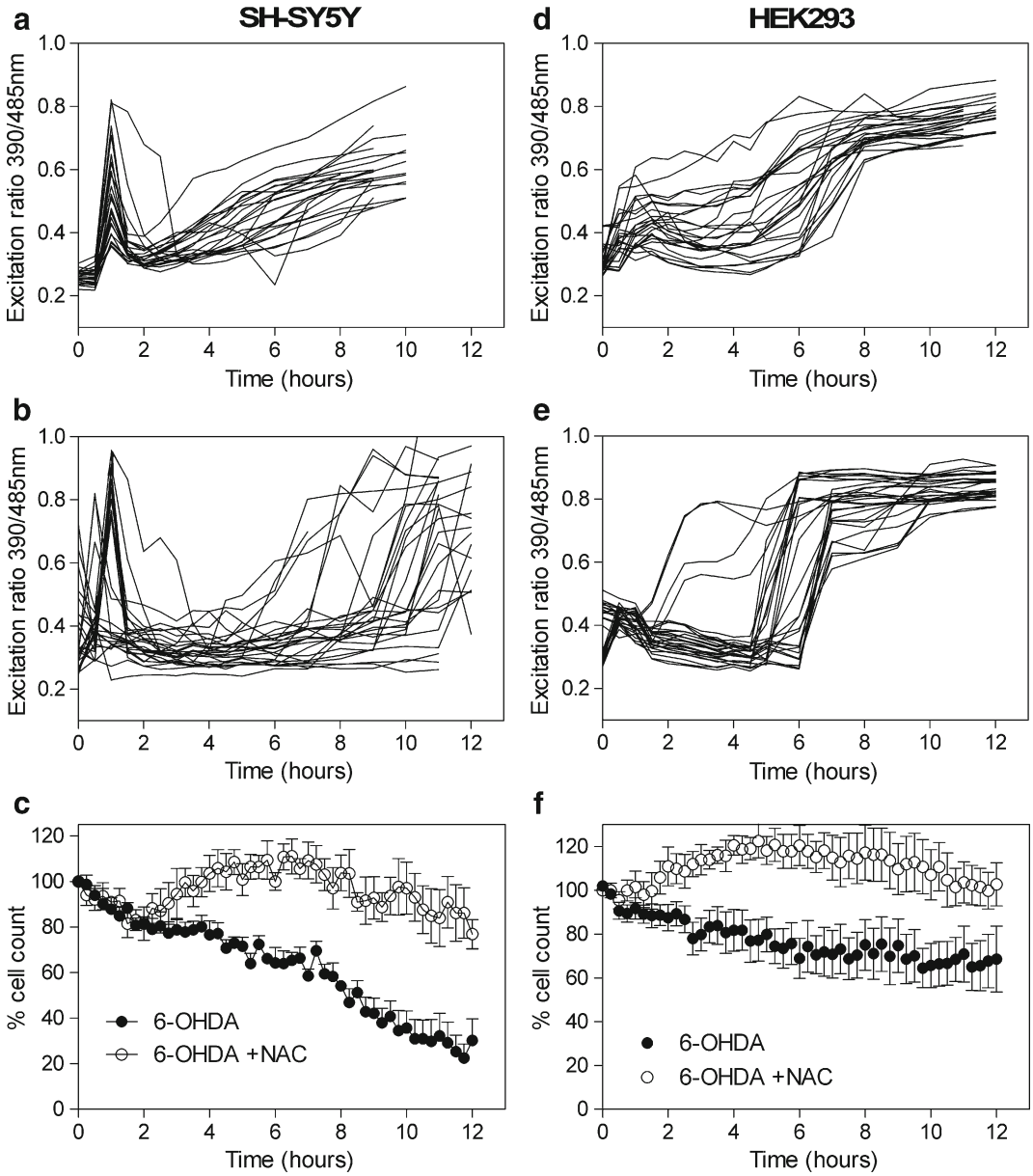

Fig. 5 Glucose starvation exacerbates the oxidative stress and cytotoxicity induced by 6-OHDA in both SH-SY5Y and HEK293 cells. SH-SY5Y cells in glucose-free media treated with **a** 6-OHDA, **b** 6-OHDA+NAC, similar treatments for HEK293 cells in (**d**) and (**e**). Ratio graphs represent the excitation ratios obtained for 20–30 individual cells from two experiments, however, each experiment was repeated in quadruplicate. Cell viability of **c** SH-SY5Y cells and **f** HEK293 cells. *Error bars* represent SEM ($n \geq 4$). *Graphs* for untreated cells provided in supplemental material

SY5Y to 6-OHDA induced an immediate transitory increase in roTurbo excitation ratio values. A similar rise and fall in ROS has been reported following 6-OHDA treatment in dopaminergic neurons labeled with fluorescent dihydroethidium, but the duration of the experiment was insufficient for a second oxidation event to be observed (Lotharius et al. 1999). A secondary and non-transitory change in ratio was observed in SH-SY5Y cells after a 4- or 5-h incubation period. Unlike the first oxidation event, which occurred at a population level, the later oxidation event was observed in single cells at different time-points.

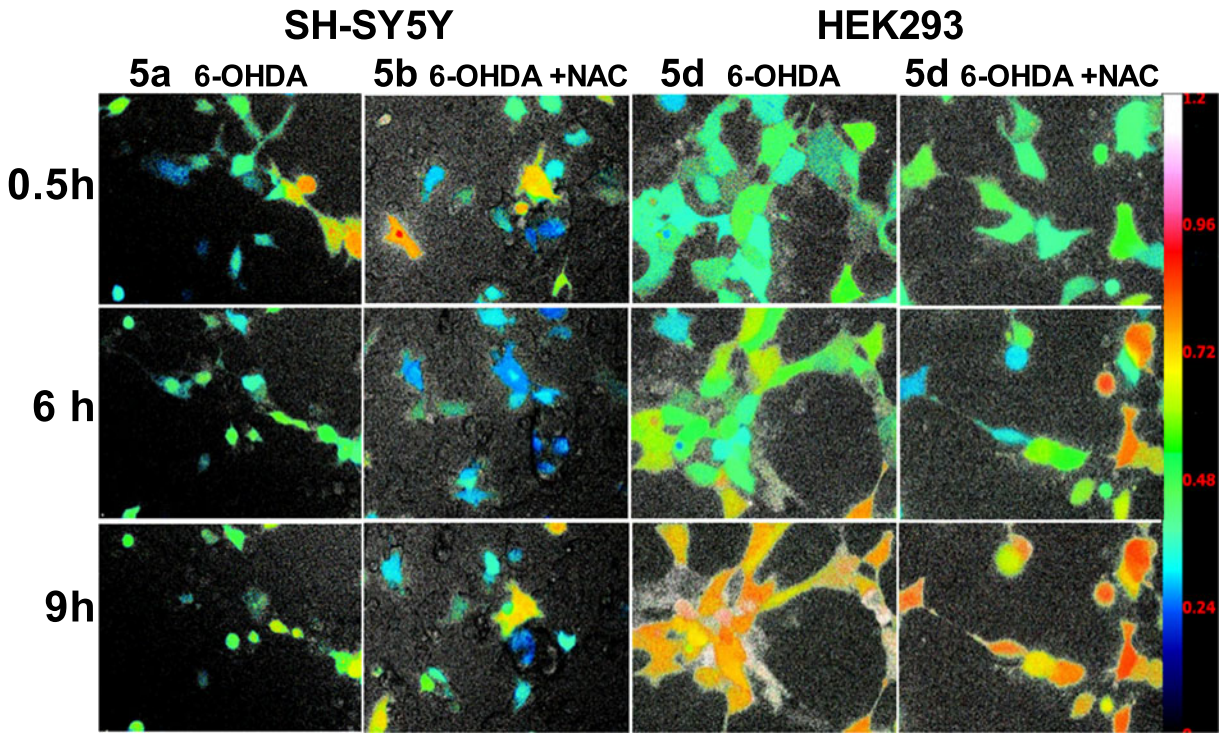

Fig. 6 Excitation ratio images of the oxidative stress induced by 6-OHDA exacerbated by glucose starvation. Images are from data graphed in Fig. 5 and have the same labels. Excitation ratio images of in SH-SY5Y and HEK293 cells in glucose-free media obtained at 0.5, 6, and 9 h. *5a* SH-SY5Y treated with 6-OHDA (100 μM) or *5b* 6-OHDA (100 μM)+NAC (10 mM), *5d* HEK293 treated with 6-OHDA (100 μM), or *5e* 6-OHDA (100 μM)+NAC (10 mM)

Demonstration that 6-OHDA induced two distinct oxidation events prompted us to inquire whether cell death could be correlated with either or both oxidative responses. We used particle analysis software (Image J, NIH, MD) to directly estimate the number of healthy fluorescent cells in the field of view throughout the experimental period. SH-SY5Y cell numbers were found to be stable in cell culture media; however, exposure to 6-OHDA resulted in a 40% to 50% decrease in cell number over the same period. Interestingly, while cell numbers did not decline until 5 h or more (a time frame similar to that observed by Jordan et al. 2004), this corresponded to the appearance of the second increase in excitation ratio. HEK293 cells exhibited a similar immediate transitional increase in excitation ratio to that in SH-SY5Y cells, but the ratio returned to near-baseline values, and cell numbers remained constant throughout the experiment.

A number of reports have described the cytotoxic effects of 6-OHDA to be primarily due to extracellularly generated ROS (Blum et al. 2001; Clement et al. 2002; Jiang et al. 2008; Soto-Otero et al. 2000), thus 6-OHDA toxicity should be similar in cells expressing (SH-SY5Y) or lacking (HEK293) monoamine transporters. The first oxidation peak occurred in all 6-OHDA-treated cell lines suggesting this oxidative event is induced by H_2O_2 produced by auto-oxidation. We compared responses of SH-SY5Y cells and HEK293 to exogenous H_2O_2. As expected, only the first oxidation peak was observed in either cell line; furthermore, there was no evidence of cell death.

In contrast, the second oxidative increase and the corresponding loss of cells were specific to the neuroblastoma cell line, supporting a cell-type-specific, and most likely an intracellular response to 6-OHDA or its metabolites. Extracellular 6-OHDA (but not H_2O_2) has been shown to activate extracellular signal-regulated protein kinases in a biphasic pattern, but activation required high concentrations and was not observed at 100 μM 6-OHDA as used in the present study (Kulich and Chu 2001). Intracellular mechanisms for 6-OHDA toxicity have been described (Brenner-Lavie et al. 2009; Chen et al. 2003; Hara et al. 2011; Lehmensiek et al. 2006; Saito et al. 2007). Our data would support the theory that while oxidative stress in response to 6-

OHDA results from both transporter-independent and transporter-dependent mechanisms, toxicity results from intracellular reactions independent of hydrogen peroxide. Cell death occurred at different times for individual cells and was never more than 60% over a 12-h period in healthy cells. This pattern of toxicity may point to a stochastic process. It was somewhat unexpected that NAC inhibited both of the 6-OHDA oxidation events and the subsequent cell loss since we could not demonstrate the NAC-quinone adduct in media; it indicates that this mechanism for toxicity can be prevented if the concentration of cytoplasmic thiols is sufficient.

When cells have limited intracellular thiol reductant available for defense against oxidative insult enhanced oxidative and toxicity responses of 6-OHDA are expected. D-glucose provides a neuroprotective effect by generation of glutathione (GSH) through the pentose phosphate pathway (PPP) (Delgado-Esteban et al. 2000) in which hexokinase (Wilson 2003) generates glucose 6-phophate from D-glucose. Two additional enzymes in the PPP use glucose 6-phosphate (Ben-Yoseph et al. 1996) to provide glutathione reductase with NADPH required for the reduction of oxidized glutathione (GSSG) to glutathione (GSH). We examined the relationship between D-glucose availability and oxidative stress in these cells by monitoring their response to 6-OHDA under glucose-free conditions. We observed a heightened initial response in the cytoplasmic oxidative state that never fully reduced to pretreatment baseline values. A second oxidation event also occurred in glucose-free conditions, but in this case, the response was observed for the population as a whole rather than in individual cells. Glucose deprivation enhanced the toxicity of 6-OHDA as described by Bellucci et al. (2008) for differentiated SH-SY5Y cells. Cell death occurred throughout this experiment, and the cells ceased regular movements within 1–2 h of 6-OHDA treatment. NAC was incapable of inhibiting oxidation under glucose-free conditions, but it delayed a second oxidative response to 6-OHDA by several hours. These results support the hypothesis that glucose plays a pivotal role in maintaining the reducing environment in cell cytoplasm and that lowered glucose levels result in a heightened response to oxidative stresses. In conditions where cells are already under oxidative stress, they may be killed by an oxidative insults of 6-OHDA that they would normally recover from.

Collectively, we have confirmed that auto-oxidation products of 6-OHDA induce oxidative stress in neuroblastoma cells. Additionally, we have shown this compound induces a secondary oxidative stress not related to H_2O_2. This second oxidation is rapid and highly correlated with cell death, and surprisingly, cells respond in an individual manner. roTurbo as a redox sensor has enabled us to monitor real-time changes in the cell oxidation state and has enabled us to investigate the apparently conflicting reports that 6-OHDA induces oxidative stress through either extracellular auto-oxidation or by intracellular mechanisms. This study also demonstrated that the ability of cells to overcome oxidative insults and the mechanism and timing of cell death can be altered dramatically by changes in the environment. Thus, the combination of the redox-sensing capabilities of roGFPs and cell population estimation has yielded insights into oxidative responses that could not be detected by studying either parameter alone.

Acknowledgments We thank to Michael Hodge for technical assistance and Dr. Ramanjaneya Mula for critical assessment of the manuscript. This work was supported by grants from the Arthritis & Chronic Pain Research Institute and the Alzheimer's & Aging Research Center and was supported by the State of Florida, Executive Office of the Governor's Office of Tourism, Trade, and Economic Development.

References

Andrew R, Watson DG, Best SA, Midgley JM, Wenlong H, Petty RK. The determination of hydroxydopamines and other trace amines in the urine of parkinsonian patients and normal controls. Neurochem Res. 1993;18:1175–7.

Bellucci A, Collo G, Sarnico I, Battistin L, Missale C, Spano P. Alpha-synuclein aggregation and cell death triggered by energy deprivation and dopamine overload are counteracted by D2/D3 receptor activation. J Neurochem. 2008;106:560–77.

Belousov VV, Fradkov AF, Lukyanov KA, Staroverov DB, Shakhbazov KS, Terskikh AV, Lukyanov S. Genetically encoded fluorescent indicator for intracellular hydrogen peroxide. Nat Methods. 2006;3:281–6.

Ben-Yoseph O, Boxer PA, Ross BD. Assessment of the role of the glutathione and pentose phosphate pathways in the protection of primary cerebrocortical cultures from oxidative stress. J Neurochem. 1996;66:2329–37.

Blum D, Torch S, Lambeng N, Nissou M, Benabid AL, Sadoul R, Verna JM. Molecular pathways involved in the neurotoxicity of 6-OHDA, dopamine and MPTP: contribution to the apoptotic theory in Parkinson's disease. Prog Neurobiol. 2001;65:135–72.

Blum D, Torch S, Nissou MF, Benabid AL, Verna JM. Extracellular toxicity of 6-hydroxydopamine on PC12 cells. Neurosci Lett. 2000;283:193–6.

Brenner-Lavie H, Klein E, Ben-Shachar D. Mitochondrial complex I as a novel target for intraneuronal DA: modulation of respiration in intact cells. Biochem Pharmacol. 2009;78:85–95.

Callio J, Oury TD, Chu CT. Manganese superoxide dismutase protects against 6-hydroxydopamine injury in mouse brains. J Biol Chem. 2005;280:18536–42.

Cannon MB, Remington SJ. Re-engineering redox-sensitive green fluorescent protein for improved response rate. Protein Sci. 2006;15:45–57.

Chalovich EM, Zhu JH, Caltagarone J, Bowser R, Chu CT. Functional repression of cAMP response element in 6-hydroxydopamine-treated neuronal cells. J Biol Chem. 2006;281:17870–81.

Chen J, Wersinger C, Sidhu A. Chronic stimulation of D1 dopamine receptors in human SK-N-MC neuroblastoma cells induces nitric-oxide synthase activation and cytotoxicity. J Biol Chem. 2003;278:28089–100.

Clement MV, Long LH, Ramalingam J, Halliwell B. The cytotoxicity of dopamine may be an artefact of cell culture. J Neurochem. 2002;81:414–21.

Curtius HC, Wolfensberger M, Steinmann B, Redweik U, Siegfried J. Mass fragmentography of dopamine and 6-hydroxydopamine. Application to the determination of dopamine in human brain biopsies from the caudate nucleus. J Chromatogr. 1974;99:529–40.

Delgado-Esteban M, Almeida A, Bolanos JP. D-Glucose prevents glutathione oxidation and mitochondrial damage after glutamate receptor stimulation in rat cortical primary neurons. J Neurochem. 2000;75:1618–24.

Dooley CT, Dore TM, Hanson GT, Jackson WC, Remington SJ, Tsien RY. Imaging dynamic redox changes in mammalian cells with green fluorescent protein indicators. J Biol Chem. 2004;279:22284–93.

Gutscher M, Pauleau AL, Marty L, Brach T, Wabnitz GH, Samstag Y, Meyer AJ, Dick TP. Real-time imaging of the intracellular glutathione redox potential. Nat Methods. 2008;5:553–9.

Halliwell B. Role of free radicals in the neurodegenerative diseases: therapeutic implications for antioxidant treatment. Drugs Aging. 2001;18:685–716.

Hanson GT, Aggeler R, Oglesbee D, Capaldi RA, Tsien RY, Remington SJ. Investigating mitochondrial redox potential with redox-sensitive green fluorescent protein indicators. J Biol Chem. 2004;279:13044–53.

Hara H, Kamiya T, Adachi T. Endoplasmic reticulum stress inducers provide protection against 6-hydroxydopamine-induced cytotoxicity. Neurochem Int. 2011;58:35–43.

Hwang C, Sinskey AJ, Lodish HF. Oxidized redox state of glutathione in the endoplasmic reticulum. Science. 1992;257:1496–502.

Isaev NK, Stelmashook EV, Dirnagl U, Plotnikov EY, Kuvshinova EA, Zorov DB. Mitochondrial free radical production induced by glucose deprivation in cerebellar granule neurons. Biochemistry (Mosc). 2008;73:149–55.

Izumi Y, Sawada H, Sakka N, Yamamoto N, Kume T, Katsuki H, Shimohama S, Akaike A. p-Quinone mediates 6-hydroxydopamine-induced dopaminergic neuronal death and ferrous iron accelerates the conversion of p-quinone into melanin extracellularly. J Neurosci Res. 2005;79:849–60.

Jiang H, Jiang Q, Feng J. Parkin increases dopamine uptake by enhancing the cell surface expression of dopamine transporter. J Biol Chem. 2004;279:54380–6.

Jiang Y, Pei L, Li S, Wang M, Liu F. Extracellular dopamine induces the oxidative toxicity of SH-SY5Y cells. Synapse. 2008;62:797–803.

Jordan J, Galindo MF, Tornero D, Gonzalez-Garcia C, Cena V. Bcl-x L blocks mitochondrial multiple conductance channel activation and inhibits 6-OHDA-induced death in SH-SY5Y cells. J Neurochem. 2004;89:124–33.

Kulich SM, Chu CT. Sustained extracellular signal-regulated kinase activation by 6-hydroxydopamine: implications for Parkinson's disease. J Neurochem. 2001;77:1058–66.

Lehmensiek V, Tan EM, Liebau S, Lenk T, Zettlmeisl H, Schwarz J, Storch A. Dopamine transporter-mediated cytotoxicity of 6-hydroxydopamine in vitro depends on expression of mutant alpha-synucleins related to Parkinson's disease. Neurochem Int. 2006;48:329–40.

Liu S, Ansari NH, Wang C, Wang L, Srivastava SK. A rapid HPLC method for the quantification of GSH and GSSG in ocular lens. Curr Eye Res. 1996;15:726–32.

Lotharius J, Dugan LL, O'Malley KL. Distinct mechanisms underlie neurotoxin-mediated cell death in cultured dopaminergic neurons. J Neurosci. 1999;19:1284–93.

Miller GM, Yatin SM, De La Garza R, Goulet M, Madras BK. Cloning of dopamine, norepinephrine and serotonin transporters from monkey brain: relevance to cocaine sensitivity. Brain Res Mol Brain Res. 2001;87:124–43.

Pedelacq JD, Cabantous S, Tran T, Terwilliger TC, Waldo GS. Engineering and characterization of a superfolder green fluorescent protein. Nat Biotechnol. 2006;24:79–88.

Saito Y, Nishio K, Ogawa Y, Kinumi T, Yoshida Y, Masuo Y, Niki E. Molecular mechanisms of 6-hydroxydopamine-induced cytotoxicity in PC12 cells: involvement of hydrogen peroxide-dependent and -independent action. Free Radic Biol Med. 2007;42:675–85.

Senoh S, Creveling CR, Udenfriend S, Witkop B. Chemical, enzymatic and metabolic studies on the mechanism of oxidation of dopamine. J Am Chem Soc. 1959;81:6236–40.

Soto-Otero R, Mendez-Alvarez E, Hermida-Ameijeiras A, Munoz-Patino AM, Labandeira-Garcia JL. Autoxidation and neurotoxicity of 6-hydroxydopamine in the presence of some antioxidants: potential implication in relation to the pathogenesis of Parkinson's disease. J Neurochem. 2000;74:1605–12.

Uttara B, Singh AV, Zamboni P, Mahajan RT. Oxidative stress and neurodegenerative diseases: a review of upstream and downstream antioxidant therapeutic options. Curr Neuropharmacol. 2009;7:65–74.

Wilson JE. Isozymes of mammalian hexokinase: structure, subcellular localization and metabolic function. J Exp Biol. 2003;206:2049–57.

Zhou C, Huang Y, Przedborski S. Oxidative stress in Parkinson's disease: a mechanism of pathogenic and therapeutic significance. Ann N Y Acad Sci. 2008;1147:93–104.

Zhu X, Su B, Wang X, Smith MA, Perry G. Causes of oxidative stress in Alzheimer disease. Cell Mol Life Sci. 2007;64:2202–10.